International Journal of Concrete Structures and Materials
Vol.1, No.1, pp.19~28, December 2007

Failure Modeling of Bridge Components Subjected to Blast Loading Part I: Strain Rate-Dependent Damage Model for Concrete

Jun Wei[1)], Russ Quintero[2)], Nestore Galati[3)], and Antonio Nanni[4)]*

(Received October 25, 2007, Accepted December 14, 2007)

Abstract : A dynamic constitutive damage model for reinforced concrete (RC) structures and formulations of blast loading for contact or near-contact charges are considered and adapted from literatures. The model and the formulations are applied to the input parameters needed in commercial finite element method (FEM) codes which is validated by the laboratory blast tests of RC slabs from literature. The results indicate that the dynamic constitutive damage model based on the damage mechanics and the blast loading formulations work well. The framework on the dynamic constitutive damage model and the blast loading equations can therefore be used for the simulation of failure of bridge components in engineering applications.

Keywords : blast loading, bridge collapse, critical charges, dynamic damage model, explicit FEM, free air explosion, progressive collapse

1. Introduction

With regards to all types of threats, explosives constitute 60 percent of terrorist attacks world wide. The Federal Highway Administration (FHWA) of the United States envisioned a multi-year program[1] that will address securing the existing infrastructure and that will lead to a new generation of bridges and structures that are resilient to this new, human threat.

To protect against terrorist bomb attacks, research and technical communities must: (1) better understand the effects of blast loads on structures (*e.g.*, bridges) by using field and laboratory experimentation; (2) validate existing computational models for the prediction of such responses; (3) develop simple design/assessment tools that practitioners and bridge operators can use to enhance the protection of both existing and new structures; and (4) develop more efficient and economical mitigation strategies that include the use of engineered materials and technologies.

The need for the protection of the civil infrastructure (specifically bridges) against blast load is not a new problem. In fact, the 1987 Structures Congress already considered the protection of the civil infrastructure against terrorist attacks to be an existing problem.[2] Indeed, much research works and design manuals have been conducted on blast loads and their effects on structures, primarily in the United States,[3] the United Kingdom,[4] and Israel.[5] Much research has also been conducted on blast effects on buildings, and much of this research can be extrapolated to the development of procedures for the design of blast resistant bridges.[6] However, in many instances, it is not feasible or even practical to implement these procedures into bridge design. A major issue in the case of bridges subjected to blast loads is that charges can easily be placed near or in contact with the structural elements, and therefore, a force- or displacement-based fragility relationship would be inaccurate.[7] Experimental and numerical finite element analysis (FEA) studies on concrete blocks subject to blast loads and fragments impact.[8] showed a localized damage at the surface of the impact zone. Micro-cracking mostly happened at a depth of approximately 120 mm (5 in.) below the surface with no concrete strength degradation below this zone.

Structural elements under close-in charge explosions are subjected to very high strain rates, in the order of 10/s to 1000/s, which will substantially modify the material properties.[9] The high-strain rate data are accounted for through the ratio between the strength of the material at dynamic loading to the one under quasi-static conditions, which is referred to as dynamic increase factor (DIF).[9] For reinforced concrete (RC) under high strain rates, the apparent strength of the materials can significantly increase. Findings show that the DIF can be up to 1.5 for reinforcing steel bars, 2.0 or more for concrete in compression, and 6.0 or more for the concrete in tension.[9-11] Donze et al.,[12] using a three dimensional discrete-element method of an unconfined concrete specimen under compression and high strain rate, showed that the strain rate dependency of the concrete material is mainly attributed to internal inertia effects.

To correctly describe the strain-rate dependency in concrete, suitable constitutive relations are necessary. Three model types are currently considered to define the constitutive relations of concrete under high strain rates:[13] (1) homogenization models, which consider the compaction of the material porosity closer to

[1)]Dept. of Mechanical and Aerospace Engineering, Arizona State University, Phoenix, AZ 85069-7100, USA.
[2)]Dept. of Civil, Architectural and Environmental Engineering, University of Missouri-Rolla, Rolla, MO 65409-0710, USA.
Structural Group, Inc., Strengthening Division, Maryland 21075, USA.
[3)]Dept. of Civil, Architectural and Environmental Engineering, University of Miami, Coral Gables, FL 33146-2509, USA. *E-mail: nanni@miami.edu*

the explosion subject to a strong hydrostatic compression; (2) tensile damage models utilizing rate dependent damage models; and (3) compression failure models combining viscoplasticity with rate dependent damage models.

In this paper, approach based on dynamic constitutive damage model is adopted for reinforced concrete (RC) structures and formulations of blast loading for contact or near-contact charges are considered and adapted from literatures firstly. The model and the formulations then are applied to the input parameters in commercial finite element method (FEM) code which is validated by laboratory blast tests of RC slabs from literature. Finally, the model and the formulations will be used for the simulation of failure of bridge components in its companion paper.

All simulations have been carried out using the commercial ABAQUS/Explicit FEA code, which is an explicit dynamic finite element program. This program allows obtaining the structure's dynamic response by direct time integration of all the degrees of freedom of the model.[14,15] This program also has the capability to simulate blast load by applying an incident load condition given the geometric data describing an incident wave (*i.e.,* the standoff point coordinates), the incident wave source coordinates, the properties of the fluid that the incident wave will be traveling through, and the time-history overpressure caused by the explosion. Given the incident wave loading, ABAQUS uses an internal algorithm to accounts for the incident angle effect. The time-history overpressures for the analyses have been obtained in advance by using the closed form solutions described in the following section. ABAQUS was chosen over other FEM codes since it is able to obtain more stable results for dynamic analysis.[16]

The numerical tools described in this paper were then used for the assessment of the capacity of the primary structural elements (*e.g.,* deck, pier, and arch) of one of the two bridges of the Tenza Viaduct in Salerno, Italy, and described in companion paper.[17] It is worth to note that the current dynamic damage mechanics based material model and blast loading equations are applied on only primary structural components since the simulations were carried out using a personal computer, and therefore with a significant limitation of computing tools. This research work demonstrated how common numerical tools, often found in practice, can be used to accurately describe a very complex phenomenon.

2. Constitutive damage model

This section describes the models used for both concrete and reinforcing steel bars as input to the FEM models. Given the compressive strength of concrete, simplified constitutive equations of strain-rate dependence under compression and tension of concrete were created in a step-by-step fashion. The strain-rate dependent equations were then used in a damage mechanics model to create the concrete constitutive equations. For the steel bars, simplified elastic-perfectly plastic constitutive laws were used to reduce computational times while obtaining significant results.

2.1 Dynamic compressive strength of concrete

For each given strain rate, the dynamic compressive strength was estimated following the Comité Euro-International du Béton (CEB)[18] formulation from given value of static compressive strength:

$$K_d(\dot{\varepsilon}) = f_{cd}/f_{cm} = (\dot{\varepsilon}_c/\dot{\varepsilon}_{c0})^{1.026\alpha_s} \quad \text{for } |\dot{\varepsilon}_c| \le 30 \ \ s^{-1} \tag{1}$$

$$K_d(\dot{\varepsilon}) = f_{cd}/f_{cm} = \gamma_s(\dot{\varepsilon}_c/\dot{\varepsilon}_{c0})^{1/3} \quad \text{for } |\dot{\varepsilon}_c| > 30 \ \ s^{-1} \tag{2}$$

with

$$\alpha_s = \frac{1}{5 + 9\, f_{cm}/f_{cm0}} \tag{3}$$

and

$$\log \gamma_s = 6.156\alpha_s - 2 \tag{4}$$

where

f_{cd} is the dynamic compressive strength,
f_{cm} is the mean value of static compressive strength,
$f_{cm0} = 10$ MPa (1 MPa = 145.04 psi),
$\dot{\varepsilon}_c$ = the strain rate (s^{-1}), and $\dot{\varepsilon}_{c0} = -30 \times 10^{-6} s^{-1}$.

2.2 Dynamic compressive concrete stress-strain relations

The dynamic concrete compressive stress-strain relationship was determined by adopting the Mendis approach originally developed for high strength concrete.[19,20] The stress-strain curve used in this study includes a parabolic ascending portion and a straight line descending branch as shown in Fig. 1. Eq. (5) gives the parabolic ascending portion of the curve:

$$f = K_d f_{cm}\left[\frac{2\varepsilon}{\varepsilon_{cd}} - \left(\frac{\varepsilon}{\varepsilon_{cd}}\right)^2\right] \quad \text{for } \varepsilon \le \varepsilon_{cd} \tag{5}$$

The linear descending portion of the stress-strain relation is obtained as follows:

$$f = K_d f_{cm}[1 - Z_d(\varepsilon - \varepsilon_{cd})] \ge f_{res} \quad \text{for } \varepsilon > \varepsilon_{cd} \tag{6}$$

The residual stress, $f_{res,}$ is defined as follows:

$$f_{res} = K_d f_{cm}(0.28 - 0.0032 f_{cm}) \ge 0 \tag{7}$$

where

$$Z_d = \frac{0.5 K_d Z\left(\frac{\dot{\varepsilon}_c}{\dot{\varepsilon}_{c0}}\right)^{-\alpha}}{\frac{3 + 0.29 f_{cm}}{145 f_{cm} - 1000} - \varepsilon_{cd}} \ge 0 \tag{8}$$

$$\varepsilon_{cd} = (0.24 K_d^3 + 0.76)\,\varepsilon_c \tag{9}$$

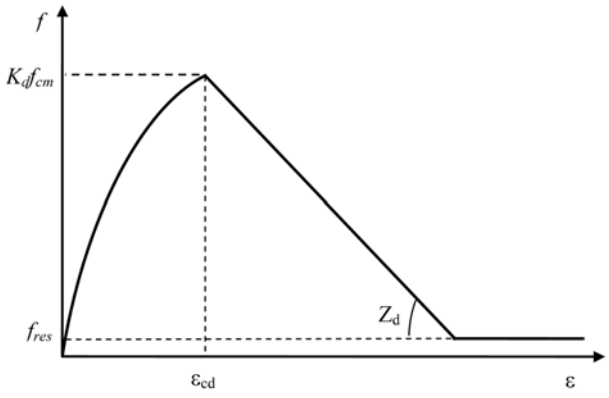

Fig. 1 Simplified dynamic stress-strain relationship of concrete.

$$Z = 0.018 f_{cm} + 0.55 \tag{10}$$

$$\varepsilon_c = \frac{4.26 f_{cm}}{\sqrt[4]{f_{cm} E_c}} \tag{11}$$

$$E_c = 4733 \sqrt{f_{cm}} (\text{MPa}) \tag{12}$$

Note that α will be calibrated with dynamic test data. As shown in Eq. (12), the value for the elastic modulus of the concrete, E_c, was assumed as the one prescribed by ACI -318-02.[21] Eq. (12) from ACI[21] results in a very close value to one from the equation recommended by [19], while the corresponding equation from CEB[18] gives about 19 percent higher. Therefore, Eq. (12) from ACI[21] is chosen in this study. Also note that the actual value for the residual strength, f_{res} should be zero. From a numerical point of view, such value cannot be assumed as zero since it would generate numerical instability. Mendis et al.[19] showed that this damage model leads to good load predictions.

2.3 Dynamic tensile strength of concrete

For a given strain rate in the range of 10^{-6} to 160 s^{-1}, the formulations of dynamic tensile strength proposed by Malvar and Ross[22] modified from Comité Euro-International du Béton (CEB)[18] was used in this research project. The corresponding dynamic tensile concrete strength is presented in Eqs. (13) and (14) starting with the static compressive strength.

$$f_{td} / f_{tm} = (\dot{\varepsilon}_t / \dot{\varepsilon}_{t0})^{\delta_s} \quad for \quad |\dot{\varepsilon}_t| \le 1 \ s^{-1} \tag{13}$$

$$f_{td} / f_{tm} = \beta_s (\dot{\varepsilon}_t / \dot{\varepsilon}_{t0})^{1/3} \quad for \quad |\dot{\varepsilon}_t| \ge 1 \ s^{-1} \tag{14}$$

with

$$\delta_s = \frac{1}{1 + 8 f_{cm} / f_{cm0}} \tag{15}$$

$$\log \beta_s = 6\delta_s - 2 \tag{16}$$

where

f_{td} = the dynamic tensile strength,
f_{cm} = the mean value of static compressive strength,
f_{cm0} = 10 MPa (1 MPa = 145.04 psi),
$\dot{\varepsilon}_t$ = the tensile strain rate in the range of 10^{-6} to 160 s^{-1}, and
$\dot{\varepsilon}_{t0} = 10^{-6} s^{-1}$.

2.4 Dynamic tensile concrete relations

For concrete subjected to tensile dynamic loading, a two-section model from CEB-FIP 90[18] was adopted. For un-cracked concrete subjected to dynamic loading, a linear stress-strain relationship is assumed as follows:

$$f_t = E_c \varepsilon_t \tag{17}$$

where

f_t = the tensile stress,
ε_t = the tensile strain, and
E_c = the tangent modulus of elasticity.

For cracked concrete sections, a fracture energy based bilinear stress-crack opening relationship (see Fig. 2) is used because it can lead to stable numerical results.[14,18]

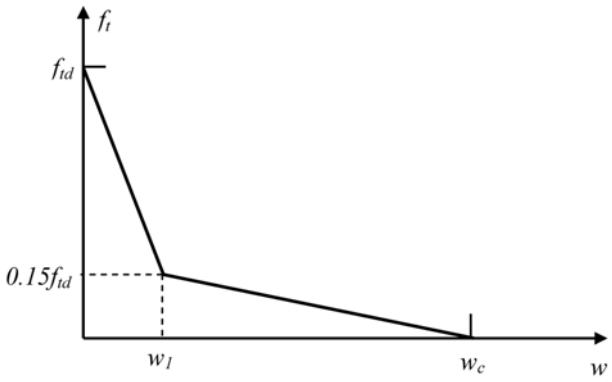

Fig. 2 Stress-crack opening diagram of concrete.

$$f_t = f_{td}\left(1 - 0.85 \frac{w}{w_1}\right) \text{ for } 0.15 f_{td} \le f_t \le f_{td} \tag{18}$$

$$f_t = \frac{0.15 f_{td} (w_c - w)}{w_c - w_1} \text{ for } 0 \le f_t \le 0.15 f_{td} \tag{19}$$

$$w_1 = 2 G_{Fd} / f_{td} - 0.15 w_c \tag{20}$$

$$w_c = \alpha_F G_{Fd} / f_{td} \tag{21}$$

where

w = the crack opening (mm, 1 mm = 0.039 inch),
w_1 = the crack opening (mm, 1 mm = 0.039 inch) for $f_t = 0.15 f_{td}$,
w_c = the crack opening (mm, 1 mm = 0.039 inch) for $f_t = 0$,
f_{td} = the dynamic tensile strength (MPa, 1 MPa = 145.04 psi),
α_F = the coefficient as given in Table 1, and
G_{Fd} = the dynamic fracture energy (Nmm/mm^2, 1 N-mm/mm^2 = 68.52 ft-lb/ft^2).

The dynamic fracture energy of concrete G_{Fd} can be defined as the energy required to propagate a tensile crack of unit area. Because of the absence of experimental data on G_{Fd}, the static equation recommended by CEB-FIP[18] was adapted to the dynamic case as follows:

$$G_{Fd} = G_{F0} (f_{cd} / f_{cd0}) \tag{22}$$

where

f_{cd0} = 10 MPa (1 MPa = 145.04 psi),
G_{F0} = the base value of fracture energy that depends on the maximum aggregate size, and d_{max} = given in Table 1.

2.5 Damage based model for concrete

For each strain rate, a damage mechanics-based concrete damage plasticity model was used in the local components' damage analysis that is subjected to blast loading.[14,15,23] The model assumes that the uniaxial tensile and compressive response of concrete is characterized by damage plasticity as shown schematically in Fig. 3. As shown in the figure, when the concrete specimen is unloaded from any point on the strain softening branch,

Table 1 Coefficient α_F and fracture energy G_{F0} vs. max aggregate size d_{max}.

d_{max}, mm(in.)	8(0.31)	16(0.62)	32(1.26)
α_F	8	7	5
G_{F0}, N/mm(lb/in.)	0.025(2.21e-4)	0.03(2.66e-4)	0.058(5.13e-4)

the elastic stiffness of the material will degrade. The degradation of the elastic stiffness is characterized by the damage indices d_t and d_c, characterizing the level of damage in tension and compression, respectively. The damage indices can take values from zero (representing the undamaged material) to one (representing the total loss of strength). The elastic modulus E_0 indicates the initial (undamaged) elastic stiffness of the material, and the stress-strain relations for the uniaxial tension and compression loading are given as follows:

$$\sigma_t = (1-d_t)E_0(\varepsilon_t - \tilde{\varepsilon}_t^{pl}) \tag{23}$$

$$\sigma_c = (1-d_c)E_0(\varepsilon_c - \tilde{\varepsilon}_c^{pl}) \tag{24}$$

Based on the definition, the effective tensile and compressive stresses are obtained as shown:

$$\overline{\sigma_t} = \frac{\sigma_t}{(1-d_t)} = E_0(\varepsilon_t - \tilde{\varepsilon}_t^{pl}) \tag{25}$$

$$\overline{\sigma_c} = \frac{\sigma_c}{(1-d_c)} = E_0(\varepsilon_c - \tilde{\varepsilon}_c^{pl}) \tag{26}$$

The size of the yield (or failure) surface will then be determined via the effective stresses.

2.6 Dynamic stress-strain relations for steel bars

To simplify the problem and reduce the computational times, an idealized characteristic of steel rebar was used in this study. This idealized characteristic is according to CEB-FIP[18] in which E_s indicates the modulus of elasticity, and f_y denotes the yield stress.

The hardening property for steel bars can also be considered in modeling the reinforcement. For this study, the authors preferred to use the simplified idealized property from CEB-FIP MODEL CODE 1990[18] to reduce computational times, yet obtaining at the same time, conservative results. In this perfect plastic model of steel confinements, the Young's modulus is assumed as independent to the strain rate, while the yield strength in dynamic loading was assumed to be 1.5 times the static one.[7,10]

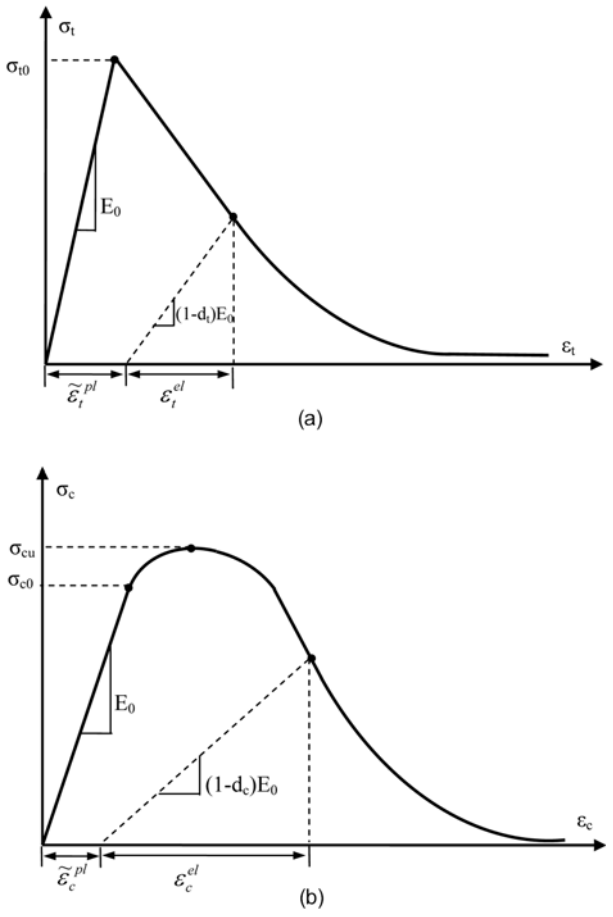

Fig. 3 Response of concrete to uniaxial loading in tension (a) and compression (b).

3. Blast loading

In this section, blast loading equations for free-air explosions are described first. Based on these equations, some special cases of explosions, contact charges and charges on the ground or on the surface of bridge, will be extended to study bridge components under explosive loads. More details on the applications of the special cases of explosion are presented in the companion paper.[17]

3.1 Free air explosion

A bomb burst can be defined as a very rapid release of stored energy characterized by an audible blast. A major part of the energy is transmitted via shock wave through the surrounding air at a supersonic velocity. The explosive blast wave has an instantaneous rise, a rapid decay, and a relatively short duration. A typical pressure-time history for a charge burst wave is shown in Fig. 4. As shown in the figure, the overpressure reaches atmospheric pressure and then falls below it in a short time. An empirical quasi-exponential form can be used to describe a free-air explosion wave of the positive phase of a spherical chemical charge [24]

$$P(t) = P_0(1 - t/t_d)e^{-\alpha t/t_d} \tag{27}$$

where

$P(t)$ = the instantaneous overpressure at time t,
P_0 = $(P_m - P_a)$ is the maximum or peak overpressure observed when t is zero,
P_a = atmospheric pressure,
P_m = the peak pressure when t is zero,
e = the base of natural logarithms,
α = the decay factor, and
t_d = the positive pressure duration.

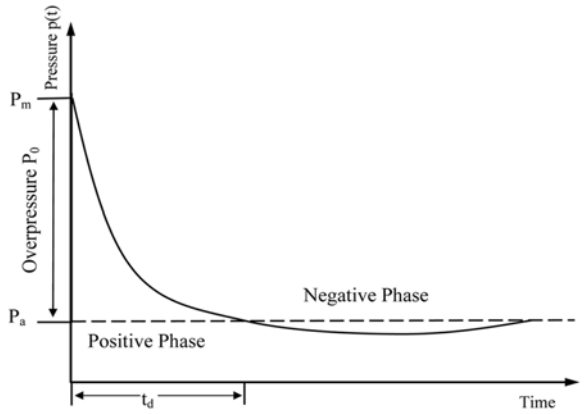

Fig. 4 A typical pressure-time curve for an explosive blast wave.

Since the positive phase of an explosion causes most of the damage for heavy structures,[24-26] the blast load parameters are defined in this project in reference to the positive phase.

In Eq. (27), the overpressure P_0 in Pascal (1 Pa = 1.45E-4 psi) is calculated by [24].

$$P_0 = \frac{808P_a\left[1+\left(\frac{Z}{4.5}\right)^2\right]}{\sqrt{1+\left(\frac{Z}{0.048}\right)^2}\sqrt{1+\left(\frac{Z}{0.32}\right)^2}\sqrt{1+\left(\frac{Z}{1.35}\right)^2}} \quad (28)$$

in which, the atmospheric pressure, P_a, is taken as 0.10132 MPa (14.7 psi). The positive loading duration in milliseconds is expressed as follows[24]:

$$t_d = \frac{980W^{1/3}\left[1+\left(\frac{Z}{0.54}\right)^{10}\right]}{\left[1+\left(\frac{Z}{0.02}\right)^3\right]\left[1+\left(\frac{Z}{0.74}\right)^6\right]\sqrt{1+\left(\frac{Z}{6.9}\right)^2}} \quad (29)$$

The decay factor a is available in [24] with tabulated data varying with scaled distance Z. For an efficient application of Eq. (27) to the computer simulating, α is fitted to an equation as function of Z as in Eq. (30). Considering the application of the blast loadings are mostly the close-in cases in this study, the scaled distance Z could be small, therefore Z is fitted within a range of 3 to get more accurate equation. The relative coefficient, R-squared value, of this fitting reaches 0.9998. It should be noted that the maximum value of a is 4 tabulated in [24] corresponding to Z equals to 0.952. In some applications, if Z is less than this value, an extrapolation is needed to get corresponding value of α by using Eq. (30).

$$\alpha = 0.3306Z^4 - 3.1838Z^3 + 11.755Z^2 - 20.308Z + 15.12, \quad \text{for } Z < 3.0 \quad (30)$$

Z is the scaled distance:

$$Z = d \times W^{-1/3} \quad (31)$$

where W is the charge weight in kilograms (1 kg = 2.2 lb), and d is the standoff distance in meters (1 meter = 3.28 feet). The reflection coefficient is as follows[24]:

$$R_c = \frac{8P_0 + 14P_a}{P_0 + 7P_a} \quad (32)$$

Therefore, the dynamic pressure, $P_d(t)$, imposed on the surface of a structure can be expressed as follows:

$$P_d(t) = R_c P_0 (1 - t/t_0) e^{-at/t_d} \quad (33)$$

Normally, the incident angle or reflect angle of the blast loading incident wave affects the structural loading conditions. In this research project, a spherical incident wave loading was used, the effect of the incident angle or reflect angle is accounted in the ABAQUS algorithm.

3.2 Contact charges

Since most terrorist attacks to a bridge structure would consist of charges close to the elements (*e.g.*, piers, arch, and the bridge deck), the case of contact charges must be considered. Assuming a spherical shape for the explosive, the charge can be considered to be in contact when the distance between the center of the explosive and the target surface is less than or equal to twice its radius (see Fig. 5). The diameter of the spherical charge can then be defined as the distance between the center of the explosive and the target surface, and it can be calculated as a function of the charge size as shown in the following equation:

$$d = 2r = \left(\frac{6W}{\pi d_{en}}\right)^{1/3} \quad (34)$$

where W represents the weight of the charge, and d_{en} the corresponding density. Substituting Eq. (34) into Eq. (31) leads to the following equation:

$$z = \left(\frac{6}{\pi d_{en}}\right)^{1/3} \quad (35)$$

Eq. (35) shows that, for charges placed in contact with the element, the scale distance becomes independent from its size. Consequently, the weight of contact charges will have an effect on the loading duration, t_d, given by Eq. (27), without affecting the overpressure P_0 and the decay factor a. Eq. (35), together with Eqs. (27) through (33), were used in the FEM model to characterize the loading conditions corresponding to this case.

3.3 Charge on ground

The case of explosions on ground may be significant in the case of on the surface of the bridges, especially for decks where the charge can be driven onto the bridge. Since for this loading case, the energy is concentrated into a hemisphere instead of being dispersed in three dimensions, the effective charge could be twice the original weight.[24] Considering the energy losses from the crater formation on the yielding surface during bursting, a conversion factor equal to 1.8 was taken.[26,27] The case of a charge on the ground was then studied by using the effective charge weight in Eqs. (27) through (33).

4. Validations

The validation of the numerical model adopting the introduced dynamic constitutive damage model and assumed blast loading formulations was performed by comparing the numerical results based on FEM simulations with experimental results obtained on RC slabs subject to close-in blast loads.[28] Such tests were performed at the University of Missouri-Rolla as part of a companion experimental campaign.

4.1 Blast test of RC slab

The validation of the numerical model was performed on RC

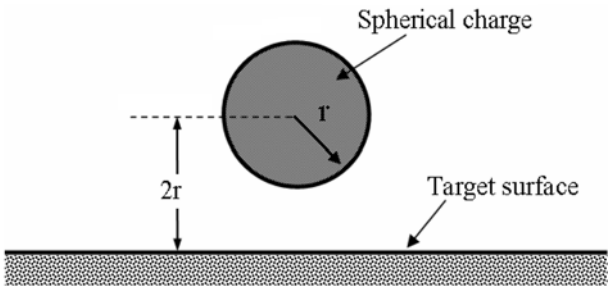

Fig. 5 Sketch showing the contact charge location.

slabs 1.22 × 1.22 × 0.089 m (48 × 48 × 3.5 in) in size, reinforced with steel bars uniformly placed in both directions as positive reinforcement, and with a clear cover of 13 mm (0.5 in) from the bottom surface. The same amount of steel reinforcement was used in both directions, consisting of ribbed steel bars having cross-sectional areas of 71 mm^2 (0.11 in^2) and spaced 152 mm (6 in) on center. The slab rested on 2 parallel "I" beams having 0.152 m (6 in.) wide flanges without anchors as shown in Figs. 6 and 7. The charge was hung above the slab center. The charge weight (W) and standoff distance (d) of two blasting cases are listed in Table 2, such that the free-air blasting equations are used in these simulations because there is a distance between the charge and the target. Due to the limitation of recording devices for the explosion test, the test results are referred to post-test photographs from the observed damage pattern. The damage levels observed from the tests are listed in Table 2, and the corresponding damage patterns are shown in Figs. 6 and 7, respectively. In Table 2, the major crack indicates the observed millimeters-wide visible cracks and the severe damage indicates complete crushing of concrete and large permanent deformation of the steel refinements as shown in Figs. 6 and 7, respectively.

The static compressive strength of the concrete used in these tests was 30.3 MPa (4.4 ksi). Following the procedures described in the previous section 2, the dynamic material properties and corresponding input parameters for the concrete and the steel were obtained via the static compressive strength. The dynamic properties of concrete at a strain rate of 100/s are as follows: Young's modulus = 26,100 MPa (3,780 ksi), Poisson's ratio = 0.2, compressive failure stress = 70.3 MPa (10.2 ksi), strain at failure = 4.76eE-3, tensile failure stress = 19.8 MPa (2.8 ksi), shear dilatation angle = 36.31°, and ratio of biaxial to uniaxial compressive failure stress = 1.16 the last two parameters are used from ABAQUS default parameters. The dynamic properties of the steel reinforcement are as follows: Young's modulus = 200 GPa (2.9E4 ksi), Poisson's ratio = 0.3, and yield stress = 388 MPa (56.3 ksi) at strain rate 1e-4/s and = 547 MPa (79.4 ksi) at strain rate 174/s. The blast loading parameters, overpressure P_0, loading duration t_d and decay factor a, of two cases are listed in Table 2 following

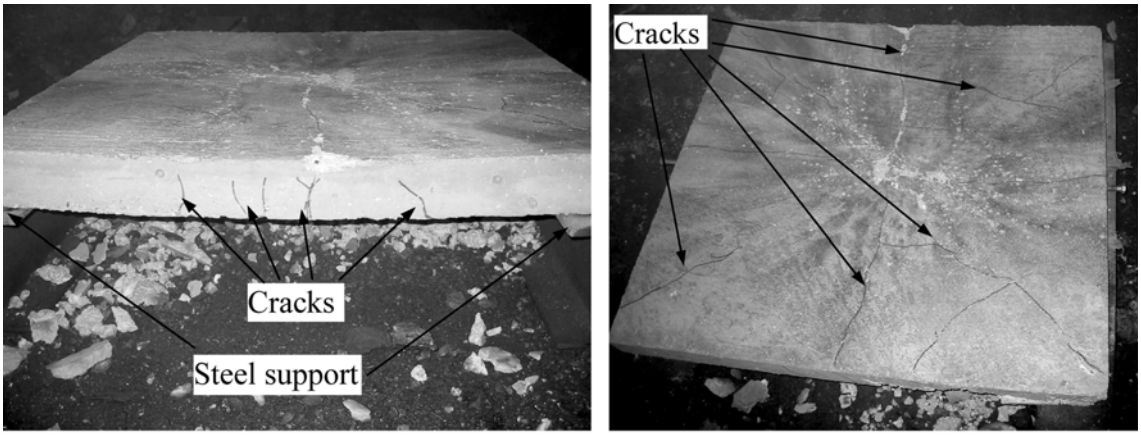

Fig. 6 Experimental results of RC slab under case 1.

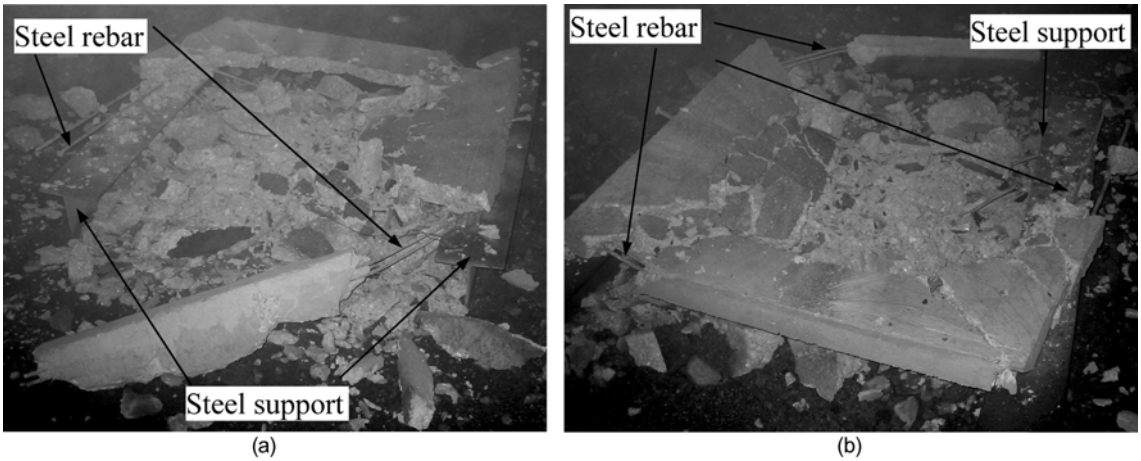

Fig. 7 Damage patterns of experimental results of RC slab under case 2.

Table 2 Blast test results and the corresponding blast loading parameters.

Case	Damage level	W, kg(lb)	d, m(in)	P_0, MPa(psi)	t_d, ms	α
1	Major cracking	1.16(2.5)	0.3(12.0)	10.4(1513)	0.41	10.3
2	Severe damage	1.71(3.8)	0.2(8.0)	20.9(3032)	2.42	12.2

the calculating procedure in section 3.

The parameters listed above were used as input for FEM. It should be noted that a strain rate of 100/s is assumed for whole slab even though somewhere off centering of the target center may subjected to low strain rate.

4.2 Simulations using FEM

The two cases were simulated using ABAQUS/Explicit FEA codes. Only a quarter of the slab was modeled because of structural and geometrical symmetry. Since the explosive charges are hung close to the slab top surface, the spherical shock wave front is considered and the corresponding input parameters are use as input in the ABAQUS/Explicit FEA code. Fig. 8 shows the central deflection time history of the slab under case 1. The maximum deflection reaches 52.15 mm (2.1 in.) at 10 ms and then recovers to 44.1 mm (1.7 in.) eventually which indicates the residual deformation. The simulated cracks are shown in Fig. 9 featured with varied orientations. Some of the cracks are radial, and some are circumferential, which is consistent with the experimental results shown in Fig. 6. These cracks are mostly flexural cracks caused by the bending generated by the relative lower overpressure when the explosive charge is closely put above the center of the slab. Under case 1, the simulated crack initiation occurs at 0.18 ms as shown in Fig. 10 in which (a) shows cracks with circular ring pattern at top surface of the ground zero while (b) shows cracks corresponding to local bending and damage corresponding to spalling at the surface opposite the ground zero caused by reflection of compressive stress wave at the bottom boundary. Fig. 11 shows the minimum principal stress contours on the top surface of the ground zero starts at time 0.03 ms and the compressive stress wave propagates along radial direction finally reaches the edges forming circular rings. The minimum principal stresses are 51.4 MPa (7.46 ksi), 44.3 MPa (6.43 ksi), 43.4 MPa (6.3 ksi) and 40.8 MPa (5.93 ksi) corresponding to 0.03 ms, 0.06 ms, 0.09 ms and 0.24 ms, respectively. This is mostly caused by the effect of spherical shock wave for close-in explosion. Fig. 12 shows the maximum principal stress on the bottom surface opposite the ground zero at the same time as at Fig. 11. The maximum principal stresses are 10.1 MPa (1.47 ksi), 16.3 MPa (2.37 ksi), 18.5 MPa (2.68 ksi) and 19.2 MPa (2.79 ksi) corresponding to 0.03 ms, 0.06 ms, 0.09 ms and 0.24 ms, respectively. This positive maximum principal stress mainly caused by the reflection of the compressive stress wave on the bottom surface boundary and the local bending. In this simulation, a rebar layer was used instead of the individual rebars[14] which were provided by ABAQUS to reduce the pre-processing efforts especially for large bridge components. The membrane stress contours are shown in Fig. 13 (a) at time of 0.15 ms when yielding is beginning where the maximum tensile stress is 383.1 MPa (55.56 ksi) and the minimum tensile stress in 205.6 MPa (29.82 ksi). Fig. 13 (b) shows large area yield of the rebar layer at time of 10 ms corresponding to maximum central deflection where the maximum tensile stress is 489.4 MPa (70.98 ksi) and the minimum tensile stress in 77.43 MPa (11.23 ksi).

Fig. 14 shows the simulated damage pattern of a quarter of the slab at 1 ms in which the grey areas indicate the damage corresponding to case 2 shown in Fig. 7. The large damage area indicates the crushing of concrete caused by relatively higher blast overpressure. For the higher blast overpressure, the damage initiates at 0.07 ms as shown in Fig. 15 (a) for the compressive damage and (b) for the tensile damage which caused by the spalling on the bottom surface opposite the ground zero.

Note that the cracks are represented by very rough element meshes because of the limits of computer memory for the 3-dimensional problem; otherwise, very fine elements would be used. A good agreement between numerical and experimental

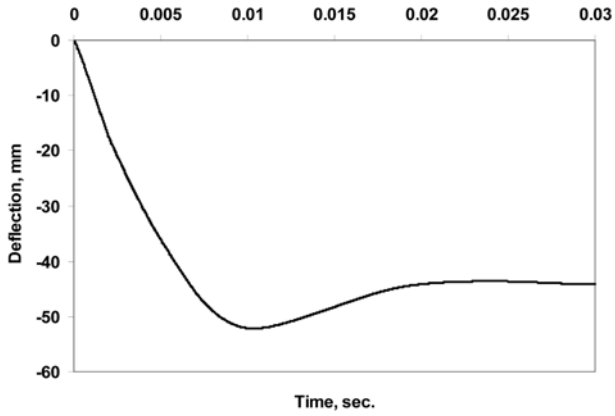

Fig. 8 Deflection time history of the slab at center under case 1.

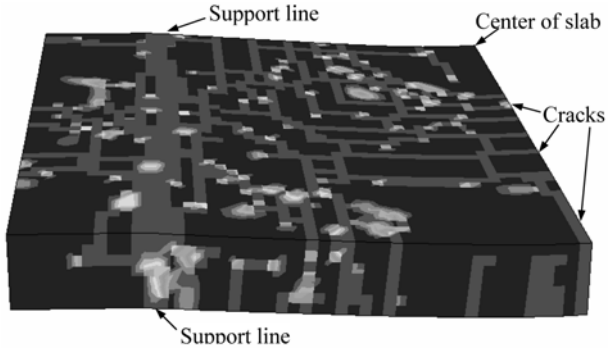

Fig. 9 Damage pattern of a quarter of the slab under case 1 at 30 ms (Grey indicates cracks).

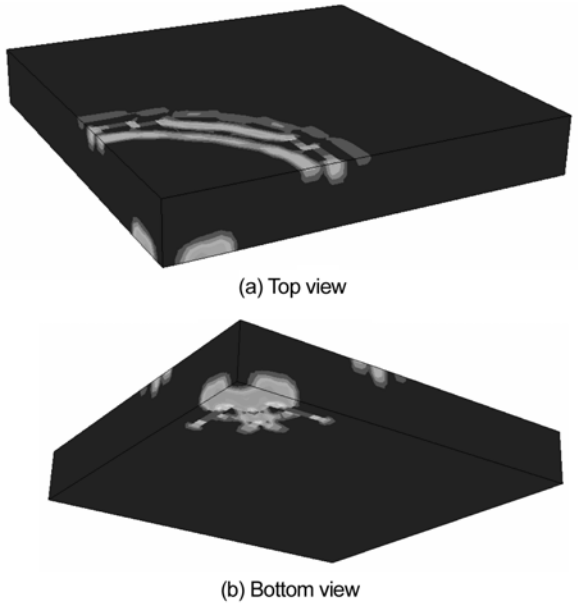

Fig. 10 Cracks initiate at time 0.18 ms under case 1.

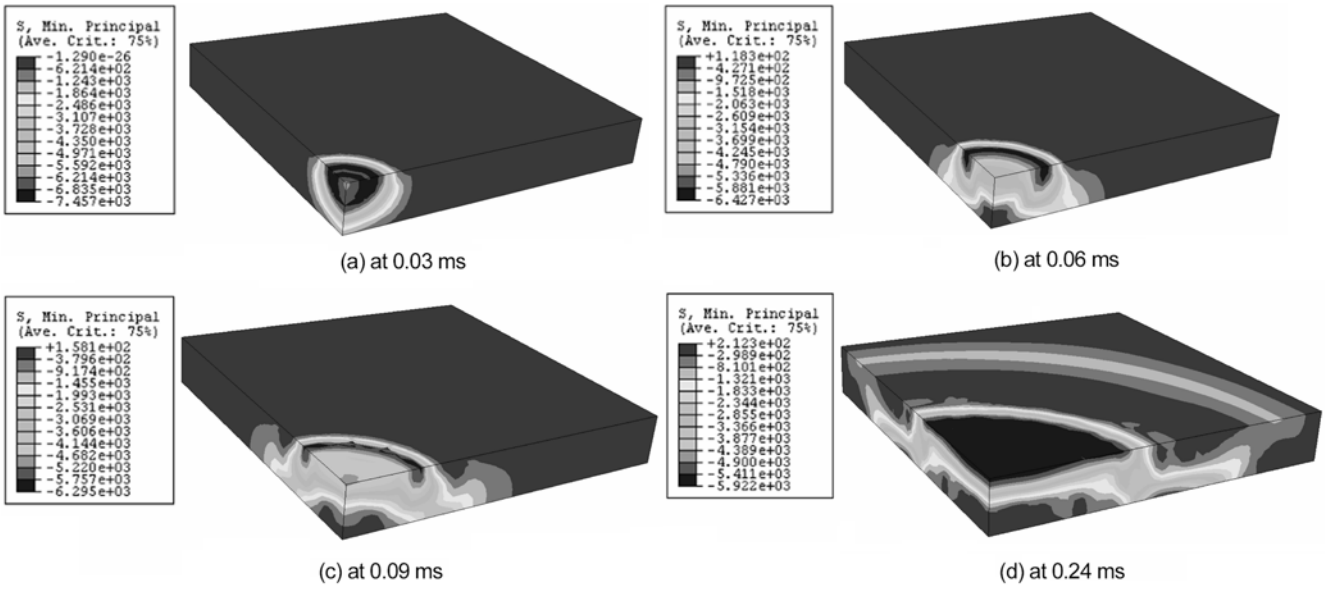

Fig. 11 Minimum principal stress contours of the slab at give time under the case 1.

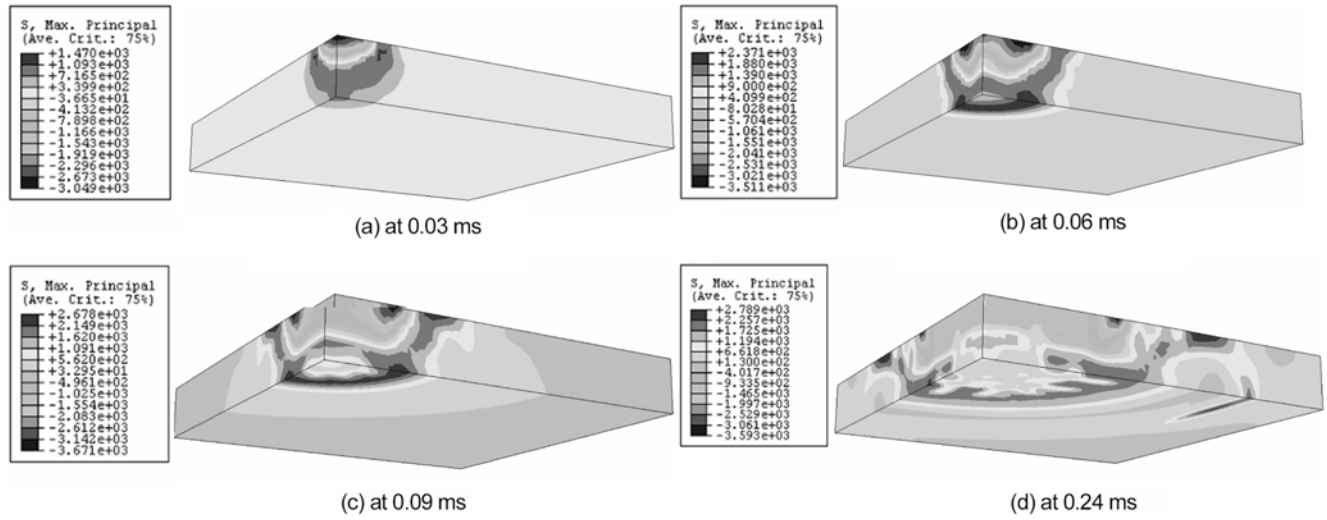

Fig. 12 Maximum principal stress contours of the slab at give time under the case 1.

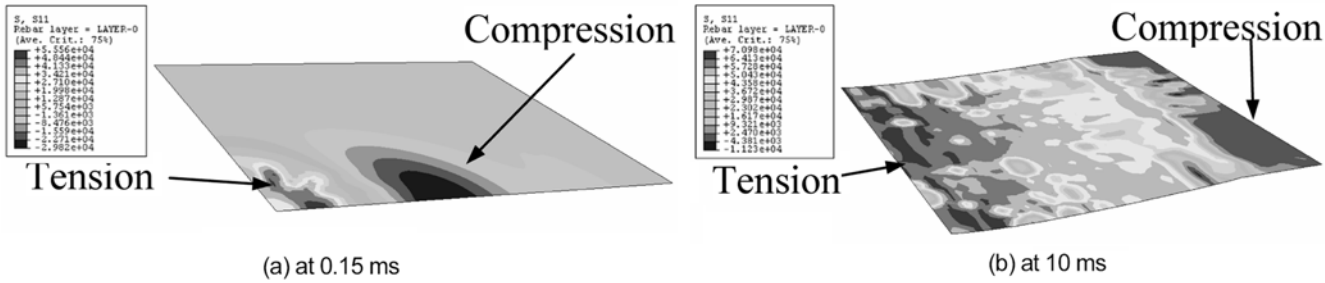

Fig. 13 Membrane stress contours of the equivalent steel rebar layer at give time under the case 1.

results was found based on the predicted damage pattern and the observations of the post-test photographs. The dynamic constitutive damage model based on the damage mechanics and the blast loading formulations is acceptable, and therefore, it was chosen for the simulation of bridge components subjected to blast loading. The results of such analysis are described in the companion paper.[17]

5. Summary

A framework of dynamic constitutive damage model for RC concrete and formulations of the blast loading were considered, adapted and validated to experimental data available in the literatures. The FEM results were compared with the laboratory blast tests of slabs. The results indicate that the dynamic constitutive

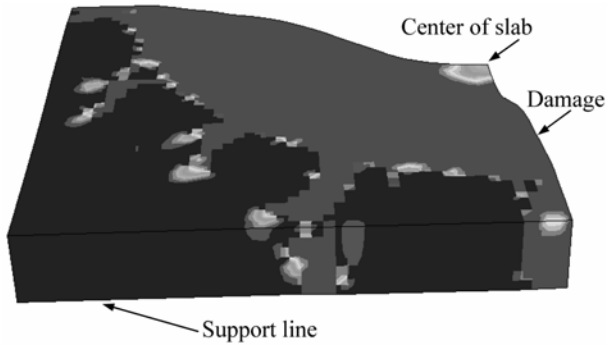

Fig. 14 Damage pattern of a quarter of the slab under case 2 at 1 ms (Grey indicates damages and cracks).

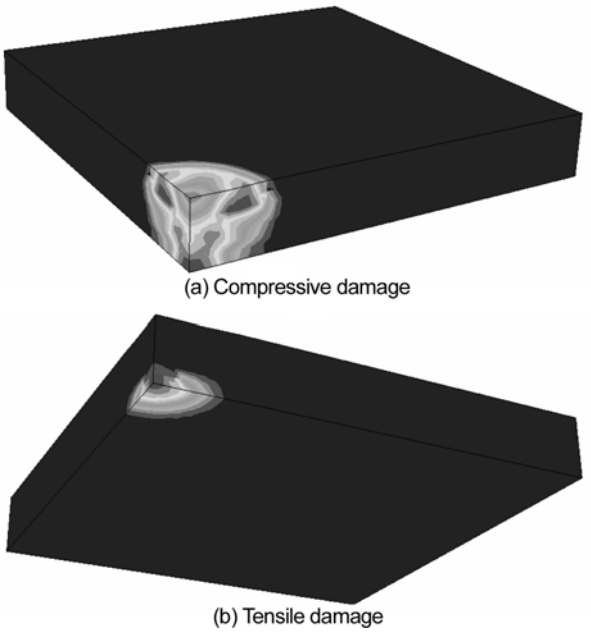

Fig. 15 0.07 ms under case 2.

damage model based on the damage mechanics and the blast loading formulations is acceptable. Therefore, the model was chosen for the simulation of failure modeling of the bridge components subjected to close-in charge blast loading.

Acknowledgments

The authors are grateful to Technical Support Working Group for funding support to this project.

Notation

d_{max} = Maximum aggregate size
d = Standoff distance of an explosion
d_{en} = Density of an explosive charge
d_c = Degradation of compressive elastic modulus of concrete
d_t = Degradation of tensile elastic modulus of concrete
e = Base of natural logarithms
f = Compressive stress
f'_c = Strength of concrete under compression
f_{cd} = Dynamic compressive strength
f_{cd0} = 10 MPa, dynamic compressive stress constant of concrete equals to 1450.4 psi
f_{cm} = Average static compressive strength
f_{cm0} = 10 MPa, static compressive stress constant of concrete equals to 1450.4 psi
f_{res} = Residual stress
f_{si} = Strength of the steel bar
f_t = Tensile stress
f_{td} = Dynamic tensile strength
f_{cm} = Average static tensile strength
f_y = Yield strength of steel
s = Time, second
t = Time, second
t_d = Positive pressure duration of a shock wave
t_{eq} = Equivalent measuring time
w = Crack opening
w_1 = Crack opening for $f_t = 0.15\, f_{td}$
w_c = Crack opening for $f_t = 0$
E_0 = Initial (undamaged) elastic modulus of concrete
E_c = Elastic modulus of concrete
E_s = Elastic modulus of steel
$P(t)$ = Instantaneous overpressure at time t
$P_d(t)$ = Dynamic pressure
P_0 = Maximum or peek overpressure observed when t is zero
P_a = Atmosphere pressure
P_m = Peek pressure when t is zero
R_c = Reflection coefficient
W = Explosive charge weight
Z = Variable or scaled distance of a explosion
Z_d = Variable
α = Coefficient of material property or decay factor of shock wave
α_F = Coefficient
G_{Fd} = Dynamic fracture energy
α_s = Variable
β_s = Coefficient
δ_s = Coefficient
γ_s = Variable
ε = Strain
ε_c = Static strain at maximum stress of concrete or compressive strain
ε_c^{el} = Compressive elastic strain of concrete
$\tilde{\varepsilon}_c^{pl}$ = Compressive plastic strain of concrete
ε_t^{el} = Tensile elastic strain of concrete
$\tilde{\varepsilon}_t^{pl}$ = Tensile plastic strain of concrete
ε_{cd} = Dynamic strain at maximum stress of concrete
$\dot{\varepsilon}$ = Strain rate (s^{-1})
$\dot{\varepsilon}_c$ = Compressive strain rate (s^{-1})
$\dot{\varepsilon}_{c0}$ = $30 \times 10^{-6}\ s^{-1}$, compressive strain rate constant of concrete
ε_t = Tensile strain
$\dot{\varepsilon}_t$ = Tensile strain rate (s-1)
$\dot{\varepsilon}_{t0}$ = $10^{-6}\ s^{-1}$, tensile strain rate constant of concrete
σ = Stress

σ_c = Compressive stress
σ_t = Tensile stress
σ_{c0} = Compressive stress at yield point
σ_{cu} = Ultimate compressive stress
σ_{t0} = Tensile stress at yield point
$\bar{\sigma}_c$ = Effective compressive stress
$\bar{\sigma}_t$ = Effective tensile stress

References

1. US Department of Transportation, *Federal Highway Administration, Multiyear Plan for Bridge and Tunnel Security Research*, Development and Deployment, Publication No. FHWA-HRT-06-072, Research, Development, and Technology, Turner-Fairbank Highway Research Center, McLean, VA, Feb. 2006.

2. Longinow, A., Krauthammer, T., and Mohammadi, J., "Research Needs to Resist Terrorist Attacks - Dynamics of Structures," *Proceedings of the Structures Congress - ASCE*, Orlando, FL, Aug. 17-20, 1987, pp.712~720.

3. NAVAFAC, Joint Departments of the Army, the Navy, and the Air Force, *Structures to Resist the Effects of Accidental Explosions*, TM 5-1300/ NAVAFAC P-397/AFR 88-22, Nov. 1990.

4. Barakat, M. and Hetherington, J. G., "New Architectural Forms to Reduce the Effects of Blast Waves and Fragments on Structures," *Proceedings of the 5th International Conference on Structures Under Shock and Impact? SUSI V*, WIT Press, Wessex Institute of Technology, UK, 1998, pp.53~62.

5. Eytan, R., "Practical Methods for Increasing the Blast Resistance of Existing Buildings," *Proceedings of the 3rd International Conference on Structures Under Shock and Impact? SUSI III*, WIT Press, Wessex Institute of Technology, UK, 1994, pp.29~35.

6. Department of the Army, *Structures to Resist the Effects of Accidental Explosions*, TM5-1300, Nov. 1990.

7. Nanni. A., Asprone, D., Ayoub, A., Baird, J., Filangieri, A. Rossi, Galati, N., Prota, A., Quinterno, R., Wang, M., and Wei, J., *Blast Testing and Research? Bridge at the Tenza Viaduct*, Final Report Task 1 of TSWG Contract Number N4175-05-R-4828, University of Missouri-Rolla, Rolla, MO, USA, 2006.

8. Leppanen, J., "Experimental and Numerical Analyses of Blast and Fragment Impact on Concrete," *International Journal of Impact Engineering*, Vol.31, 2005, pp.843~860.

9. Ross, C. A., Thompson, P. Y., and Tedesco, J. W., "Split-Hopkinson Pressure-Bar Tests on Concrete and Mortar in Tension and Compression," *ACI Materials Journal*, Vol.86, No.5, 1989, pp.475~481.

10. Malvar, L. J. and Ross, C. A., "Review of Strain Rate Effects for Concrete in Tension," *ACI Materials Journal*, Vol.95, No.6, 1998, pp.735~739.

11. Brara, A., Camborde, F., Klepaczko, J. R., and Mariotti, C., "Experimental and Numerical Study of Concrete at High Strain Rates in Tension," *Mechanics of Materials*, Vol.33, 2001, pp.33~45.

12. Donze, F. V., Magnier, S. A., Daudeville, L., Mariotti, C., and Davenne, L., "Numerical Study of Compressive Behavior of Concrete at High Strain Rates," *Journal of Engineering Mechanics,* Oct. 1999, pp.1154~1163.

13. Gatuingt, F. and Pijaudier-Cabot, G., "Coupled Damage and Plasticity Modeling in Transient Dynamic Analysis of Concrete," *Int. J. Numer. Anal. Meth. Geomech*, Vol.26, 2002, pp.1~24.

14. ABAQUS, User's Manual, Version 6.5, 2005.

15. ABAQUS, Theory Manual, 1997.

16. Sabuwala, T., Linzell, D., and Krauthammer, T., "Finite Element Analysis of Steel Beam to Column Connections Subjected to Blast Loads," *International Journal of Impact Engineering*, Vol.31, 2005, pp.861~876.

17. Quintero, R., Wei, J., Galati, N., and Nanni, A., "Failure Modeling of Bridge Components Subjected to Blast Loading Part II : Estimation of the Capacity and Critical Charge for the Tenza Bridge Components," *Submitted to International Journal of Concrete Structures and Materials (IJCSM)*, Oct. 2007.

18. Comite Euro-International Du Beton, *CEB-FIP Model Code 1990*, Design Code, Thomas Telford, 1993, Trowbridge, Wiltshire, UK.

19. Mendis, P., Pendyala, R., and Setunge, S., "Stress-Strain Model to Predict the Full-Range Moment Curvature Behavior of High-Strength Concrete Sections," *Magazine of Concrete Research*, 2000, Vol.52, No.4, pp.227~234.

20. Ngo, T. D., Mendis, P. A., Teo, D., and Kusuma, G., "Behavior of High-Strength Concrete Columns Subjected to Blast Loading," *http://www.civenv.unimelb.edu.au/aptes/publications/hsc_column_blast.pdf*, Dec. 2005.

21. ACI 318-02, *Building Code Requirements for Structural Concrete(ACI 318-02) and Commentary(ACI 318R-02) - An ACI Standard*, American Concrete Institute, Farmington Hills, Michigan, 2002.

22. Malvar, L. J. and Ross, C. A., "Review of Strain Rate Effects for Concrete in Tension," *ACI Materials Journal*, Nov.-Dec., 1998, pp.735~739.

23. Lubliner, J., Oliver, J., and Onate, E., "A Plastic-Damage Model for Concrete," *International Journal of Solids and Structure*, Vol.25, 1989, pp.299~329.

24. Kinney, G. F. and Graham, K. J., *Explosive Shocks in Air*, New York, Springer-Verlag, Inc., 1985.

25. Baker, W. E., *Explosions in Air*, University of Texas Press, Austin, 1973.

26. Beshara, F. B. A., "Modeling of Blast Loading on Aboveground Structures? I. general Phenomenology and External Blast," *Computers & Structures*, Vol.51, No.5, 1994, pp.585~596.

27. HNDM-1110-1-2, *Suppressive Shields-Structural Design and Analysis Handbook*, US Army Corps of Engineers, Huntsville, AL, 1977.

28. Lu, M. B., *Application of Displacement-Based Design Method to Blast-Resistant Reinforced Concrete Structures*, Ph.D. Dissertation, University of Missouri-Rolla, Rolla, MO, 2005.